catalysts

MDPI

Article

Microwave-Assisted Furfural Production Using Hectorites and Fluorohectorites as Catalysts

Vladimir Sánchez [1], Anton Dafinov [1], Pilar Salagre [1], Jordi Llorca [2] and Yolanda Cesteros [1,*]

[1] Department de Química Física i Inorgànica, Universitat Rovira i Virgili, 43007 Tarragona, Spain
[2] Department of Chemical Engineering, Institut de Tècniques Energètiques, Universitat Politècnica de Catalunya, 08028 Barcelona, Spain
* Correspondence: yolanda.cesteros@urv.cat

Received: 26 July 2019; Accepted: 20 August 2019; Published: 23 August 2019

Abstract: It has previously been reported that the use of microwave heating, together with the presence of co-solvents, improves the efficiency of furfural production from biomass. Solid acid catalysts can be a good alternative to mineral acids, since they can prevent corrosion and can be reused. However, the formation of humines should be minimized. Several delaminated and fluorinated hectorites, with different types and strengths of acid sites, were synthesized and tested as catalysts for the production of furfural from commercial xylose and from an acid biomass extract of almond shells. A new methodology was developed to prepare crystalline fluorohectorite at 800 °C in just 3 h. The presence of F significantly increased the acidity strength in the protonated fluorohectorite (H-FH) taking into account its high ammonia desorption temperature (721 °C). Additionally, this sample had fourteen times higher total acidity by m^2 than the reference H-βeta acid catalyst. H-FH was the most efficient catalyst at short reaction times (1 h) for the transformation of xylose to furfural under microwaves using toluene as co-solvent, regardless of whether the xylose was commercial (20% furfural yield) or an extract of almond shells (60% furfural yield). However, the acidity of the extract affected the fluorohectorite structure and composition.

Keywords: Green Chemistry; heterogeneous catalysis; microwaves; clays; fluorohectorite; biomass; furfural

1. Introduction

The strong dependence of society on crude oil, together with its risk of depletion, is prompting scientists to focus on research into new resources from which chemicals can be obtained. One of the most challenging goals of chemists, nowadays, is to improve furfural production from renewable lignocellulosic biomass. Furfural is considered an important building block in the chemical industry, since it can be applied for the synthesis of a vast range of chemical products [1].

Furfural can be produced by hydrolysis and subsequent dehydration of the xylan existing in large amounts in hemicellulose. The most frequently used biomass resources are agriculture wastes with high hemicellulose content, such as corncobs, oat bran, wheat bran, etc. [2]. The current furfural production from biomass is on the order of 10^5 metric tons per year [3]. Production of almonds has an important impact on the local agriculture of the Tarragona area (Catalonia). They are usually commercialized without the shell, which is burned. However, considering that the hemicellulose content of almond shells is around 30% [4], we propose revalorizing this biomass waste by producing furfural.

Brønsted acid sites play a crucial role in the dehydration of xylose towards furfural (Scheme 1), but the cooperative action of Lewis and Brønsted acid sites also showed a positive effect [5,6]. On the other hand, the formation of humines, from secondary condensation reactions with furfural, should be avoided in order to increase the furfural yield [7]. These secondary reactions can also be catalyzed by

Lewis and Brønsted acid sites, but with a higher contribution from the Lewis acid sites [5]. The current processes for obtaining furfural employs mineral acids (H_2SO_4, H_3PO_4, ...) as catalysts, resulting in environmental drawbacks due to the corrosion of the catalytic system and the low recoverability of the catalyst. This, together with the high reaction temperatures used [4], makes this method pollutant and expensive. Additionally, current yields of furfural with these homogeneous systems are relatively low (<60%) [7]. On the other hand, solid acid catalysts have been implemented for furfural production in recent years, in consideration of environmental and economic issues [8,9]. Solid acid catalysts, including zeolites, acid-functionalized MCM materials, heteropolyacids, sulfated zirconia, exfoliated titanate, niobate, and so on, exhibited higher furfural production than that homogeneous catalysts, which were also easily recovered [2,10–12].

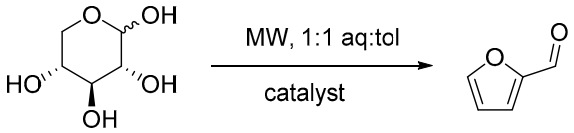

Scheme 1. General scheme for the catalytic production of furfural from xylose.

Different strategies have been proposed in the literature for improving the furfural yield. The use of microwaves to increase the heating efficiency and the use of co-organic solvents with water to favor the furfural extraction and to avoid condensation reactions improved the catalytic results [13–22]. When using homogeneous catalysts, the effect of microwaves on the increase of the furfural yield appears to be more related to the efficiency of the heating than to the direct action of the microwaves on the reaction [23]. However, the solid interface of solid catalysts could absorb microwaves, resulting in a positive action on the kinetic of the dehydration reaction [24]. Regarding the use of co-solvents, such as toluene, cyclopenthylmethylether or dimethylsulfoxide [15], toluene led to the best results, considering its price and availability [2].

There are few references concerning the use of clays for the transformation of xylose to furfural [25,26], but these materials have interesting properties that should be considered. Hectorites are clays classified as 2:1 phyllosilicates and are included in the trioctahedral smectite group, with chemical formula $M^{n+}{}_{x/n}[(Mg_{6-x}Li_x)Si_8O_{20}(OH)_4]$. The layer structure of the hectorites has two tetrahedral sheets (Si^{4+}) and a central sheet of octahedral sites (Mg^{2+} and Li^+). The negative lamellar charge generated by the partial substitution of Mg^{2+} with Li^+ in the octahedral sheet is neutralized by the presence of M^{n+} cations in the interlamellar space. When M^{n+} is a H^+, the resulting clay has Brønsted acidity. The acidity of hectorites could be improved (a) by delamination, to have higher accessibility to the acid sites [27], and (b) by the substitution of the –OH groups, defining the O_h sheet, by –F. This atom, insofar as it is more electronegative, can increase the Lewis or Brønsted strength acidity of the hectorite atoms (Mg^{2+}, Li^+ and M^{n+}), and therefore, an improvement of the acid catalysis for the xylose dehydration reaction can be expected.

In a previous work, we prepared delaminated hectorites [27]. The synthesis of fluorohectorites $Mn_{+x/n}[(Mg_{6-x}Li_x)Si_8O_{20}F_4]$ is challenging, because the –OH substitution by anion exchange in smectites is not suitable without undergoing changes in the structure. The fluorination of bentonite using a mild fluorinating reagent (HPF_6) resulted in the substantial modification of its chemical composition, with a decrease in the Si/Al ratio of around 60% [28]. Therefore, to maintain the structure, the fluorine atoms should be incorporated by synthesis. The information regarding the preparation of fluorohectorites is rather poor in the literature. The methods described involve the use of very high synthesis temperatures, e.g., at 1350 °C for 10 min [29], or temperatures of around 800–850 °C with two different routes of synthesis: the solid state at 800 °C and the liquid phase at 850 °C, which is above the melting point of lithium fluoride [30].

In this paper, we propose two main studies: the optimization of the synthesis methodology to obtain fluorohectorites, and the study of the catalytic behavior of several hectorites, with different

acidity, for the production of furfural from xylose aqueous solutions using microwave heating and toluene as co-solvent. Delaminated hectorites (Na^+ and H^+) and fluorohectorites (Li^+ and H^+) were tested as catalysts and compared with one H-beta zeolite reference catalyst. Commercial xylose and xylose solutions obtained from almond shells were used as reagents for comparison.

2. Results and Discussion

2.1. Preparation of Fluorohectorites

Our first attempt to reproduce the results of Barrer and Jones [30] consisted of performing the synthesis using commercial reagents. The XRD pattern of the sample prepared at 800 °C for 24 h showed a complex mixture of crystalline phases, which could be identified as quartz, magnesium silicates and lithium silicates. In contrast, the fluorohectorite phase was obtained together with quartz, antophyllite ($Mg_7Si_8O_{22}(OH)_2$) and some other phases for the sample prepared at 850 °C for 2 h. The presence of high amounts of quartz in both samples can be explained by the non-homogeneous mixture of the reagents. These results were not in agreement with those previously reported [30].

To improve the synthesis, we decided to increase the solid homogeneity by mixing the starting solids reagents, grounding them, and suspending the resulting solid mixture in a few milliliters of acetone. Then, the suspension was submitted to an ultrasound bath for 20 min and, finally, the solvent was evaporated. With this procedure, the fluorohectorite phase increased significantly for the sample heated at 850 °C for 2 h, but a mixture of a large number of phases still remained. For the sample prepared at 800 °C for 24 h, the fluorohectorite phase again was not detected. The thinner particles of the reagent powders should be more reactive, and therefore, the fluorohectorite phase can be easily obtained. However, the use of longer synthesis times can favor the decomposition of the fluorohectorite into other more thermodynamically favored phases.

To increase the fluorohectorite content, the behavior of the system with time was studied in more detail, and the reactivity of the reagents was controlled by sintering them before using when performing the synthesis at 800 °C. For this reason, we prepared four samples with sintered reagents at 800 °C for 3, 6, 12 and 24 h and three samples with non-sintered reagents at 850 °C for 0.5, 1 and 2 h. XRD patterns of the FH800s samples are shown in Figure 1. The main crystalline phases of all samples synthesized at 800 and 850 °C are summarized in Table 1.

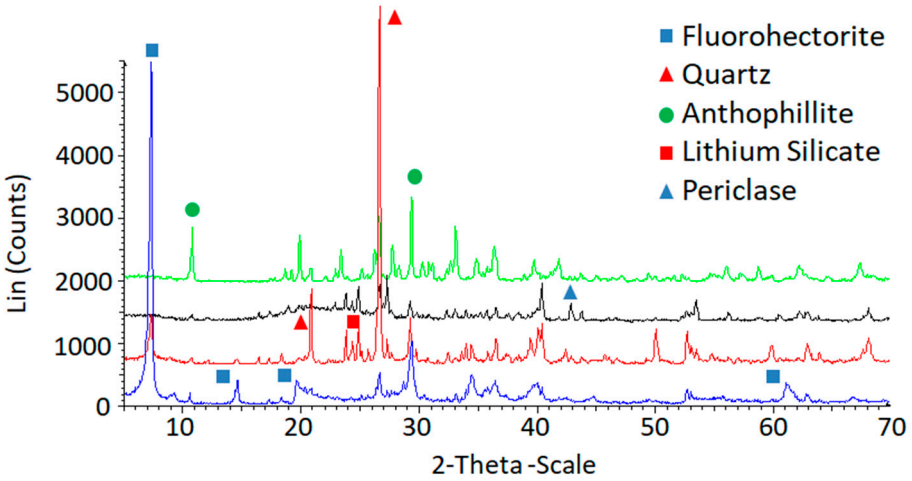

Figure 1. XRD patterns of FH800s samples synthesized at 800 °C for 3, 6 and 12 and 24 h from bottom to top.

Table 1. Phase distribution of the samples characterized by XRD.

	FH 800 °C (s)				FH 850 °C (ns)		
Synthesis Time (h)	**3**	**6**	**12**	**24**	**0.5**	**1**	**2**
Sample name	$FH800s_3$	$FH800s_6$	$FH800s_{12}$	$FH800s_{24}$	$FH850ns_{0.5}$	$FH850ns_1$	$FH850ns_2$
$Li_{0.7}(Mg_{6-x})Li_xSi_8O_{20}F_4$	**X**	X					**X**
SiO_2	X	**X**	X	X	X	**X**	X
$Li_2SiO_3/Li_2Si_2O_5$		X	X		X	X	X
MgO		X	X			X	
LiF					X	X	X
$Mg_7Si_8O_{22}(OH)_2$	X	X	X	**X**	X	X	X

Bold **X** indicates the predominant crystalline phase of the mixture. (s): sintered reagents (ns): non-sintered reagents.

Fluorohectorite was the main crystalline phase in sample $FH800s_3$, although anthophyllite and quartz were also present. This allowed us to conclude that the use of sintered reagents together with short synthesis times (3 h) at 800 °C are crucial factors in forming higher amounts of the fluorohectorite phase. Anthophyllite seems to be the most thermodynamically favored phase, since it was the main phase obtained at longer synthesis times, but it also appeared at shorter times in lower amounts. Quartz was always present: after 3 h as residual amount from the SiO_2 reagent, and after 6 h as the main phase, probably as a product of the decomposition of fluorohectorite. With respect to the experiments at 850 °C, the fluorohectorite phase was only observed in sample $FH850ns_2$ together with other phases, such as quartz, anthophyllite, lithium silicates and lithium fluoride. The best results were achieved for $FH800s_3$ and $FH850ns_2$ samples. In any case, $FH850ns_2$ showed higher complexity in its composition, indicating less purity of the material.

Based on these results, obtaining pure fluorohectorite by synthesis appears to be very difficult. Taking into account the differences in the size of the components detected in the optimized samples, we tried to purify the material after synthesis ($FH800s_3$) by centrifugation. Thus, quartz, identified by XRD, was partially separated after centrifugation at 600 rpm for 6 min. After subsequent centrifugation at 4000 rpm for 30 min, we obtained the best results for the fluorohectorite isolation. TEM image and XRD pattern of the purified material are shown in Figure 2. The characteristics of the resulting purified fluorohectorite (Li-FH) are summarized and compared with Na-delaminated hectorite (Na-DH) and H-β zeolite in Table 2.

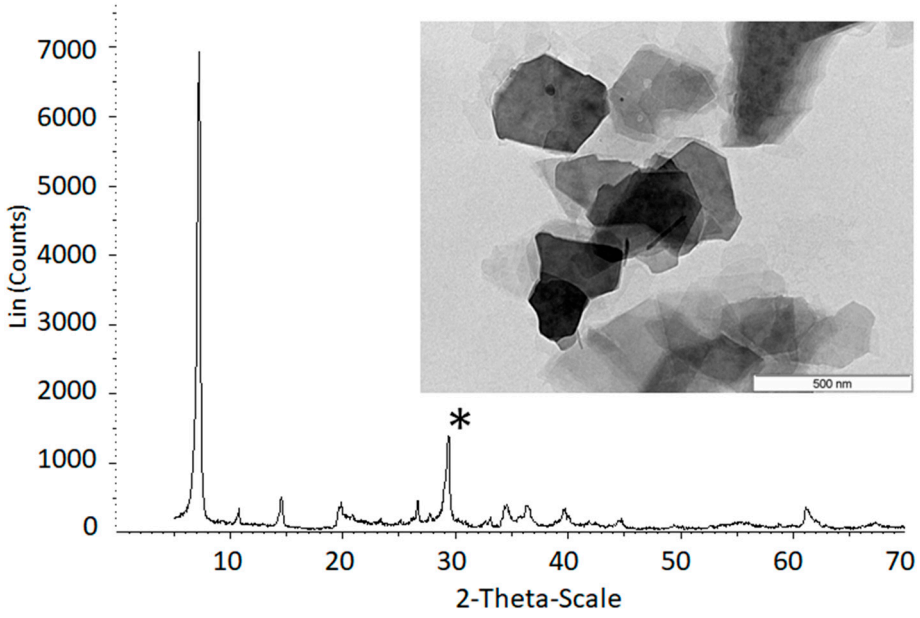

Figure 2. TEM micrograph and XRD of the purified fluorohectorite (Li-FH). * antophyllite.

Table 2. Characterization of Li-FH, Na-DH and H-β samples.

Sample	BET Area (m^2/g)	Porosity (Å)	C.E.C. (meq/100 g)	Si/F (ESEM-EDS)	Si/Mg (ESEM-EDS)
Li-FH	16	20 *, 105	105	1.8	1.5
Na-DH	327	17	60	-	-
H-β	584	17	65	-	-

* Majority pore radius.

XRD pattern of Li-FH showed a very well defined 001 reflection at 2θ = 7° corresponding to a lamellar material with high ordering in the stacking direction (Figure 2). However, some amounts of anthophyllite and a very low amount of quartz were also detected. Fluorohectorite formation was also confirmed by TEM, since well-defined but sintered lamellae with sizes between 100 and 400 nm were visualized (Figure 2). The expected presence of fibrous crystals due to anthophyllite was not observed.

EDS-SEM analysis of the Li-FH sample allowed us to confirm the presence of fluorine. Si/F atomic ratio in the purified material was 1.8 (Table 2), near the expected ratio for a totally fluorinated hectorite (theoretical value Si/F = 2). Additionally, the Si/Mg ratio of 1.5 matched the theoretical stoichiometry of the fluorohectorite $Li_{0.7}[(Mg_{5.3}Li_{0.7})Si_8O_{20}F_4]$. Lithium cannot be observed by this technique due to its small atomic number. The amount of Li was estimated in consideration of the Si/Mg ratio.

The BET surface area of Li-FH, determined by nitrogen physisorption, was low (16 m^2/g), which is in agreement with its high crystallinity and sinterization. The adsorption isotherm of this sample was mainly of type II, corresponding to non-porous materials, but with some contribution of mesoporosity related to the presence of hysteresis of type H3 according to IUPAC classification (Figure 3a) [31]. The hysteresis shape can be associated with aggregates of plate-like particles with slit-shaped pore formation. In fact, the porosity presented a bimodal distribution in which the majority of the pores had a radius of around 20 Å, but a minor part had a radius of around 105 Å (Figure 3b). The C.E.C. value of Li-FH was 105 meq/100 g, which is close to the theoretical value of 95 meq/100 g, considering the stoichiometry and expected fluorination.

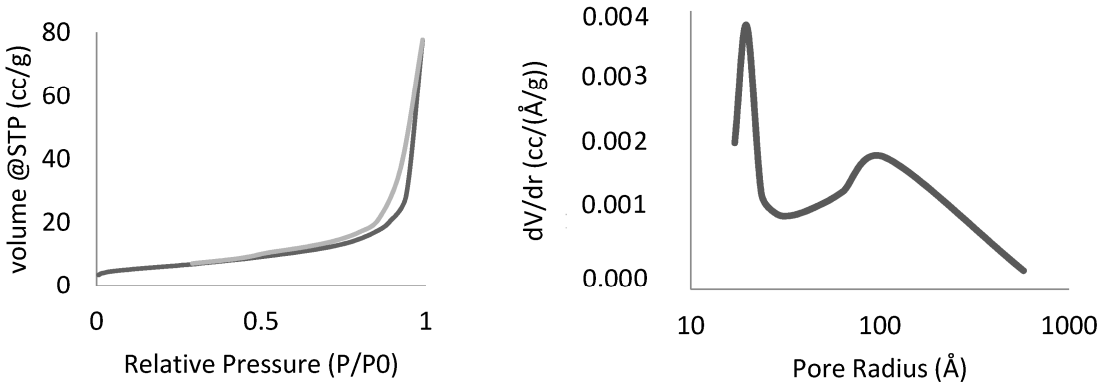

(**a**) (**b**)

Figure 3. (**a**) N_2 adsorption-desorption isotherm, and (**b**) BJH pore size distribution of fluorohectorite Li-FH.

The porosity, BET surface area and C.E.C. value of Na delaminated hectorite (Table 2) were similar to those obtained for delaminated hectorites previously prepared in the research group [27]. Fluorohectorite had much lower surface area but higher C.E.C. value than Na-DH and H-β. This will later be correlated with the catalytic results. The textural properties of the protonated forms of Li-FH and Na-DH (H-FH and H-DH) were similar to those obtained for their corresponding precursors, but significant differences in acidity should be expected.

XPS of the fluorohectorite Li-FH was performed in order to obtain information regarding the surface composition and electronic characteristics of this sample. Figure 4 shows the 2p XPS spectra for Si and Mg, and the 1s for O and F. The atomic concentration (%), binding energy values and atomic ratios are shown in Table 3.

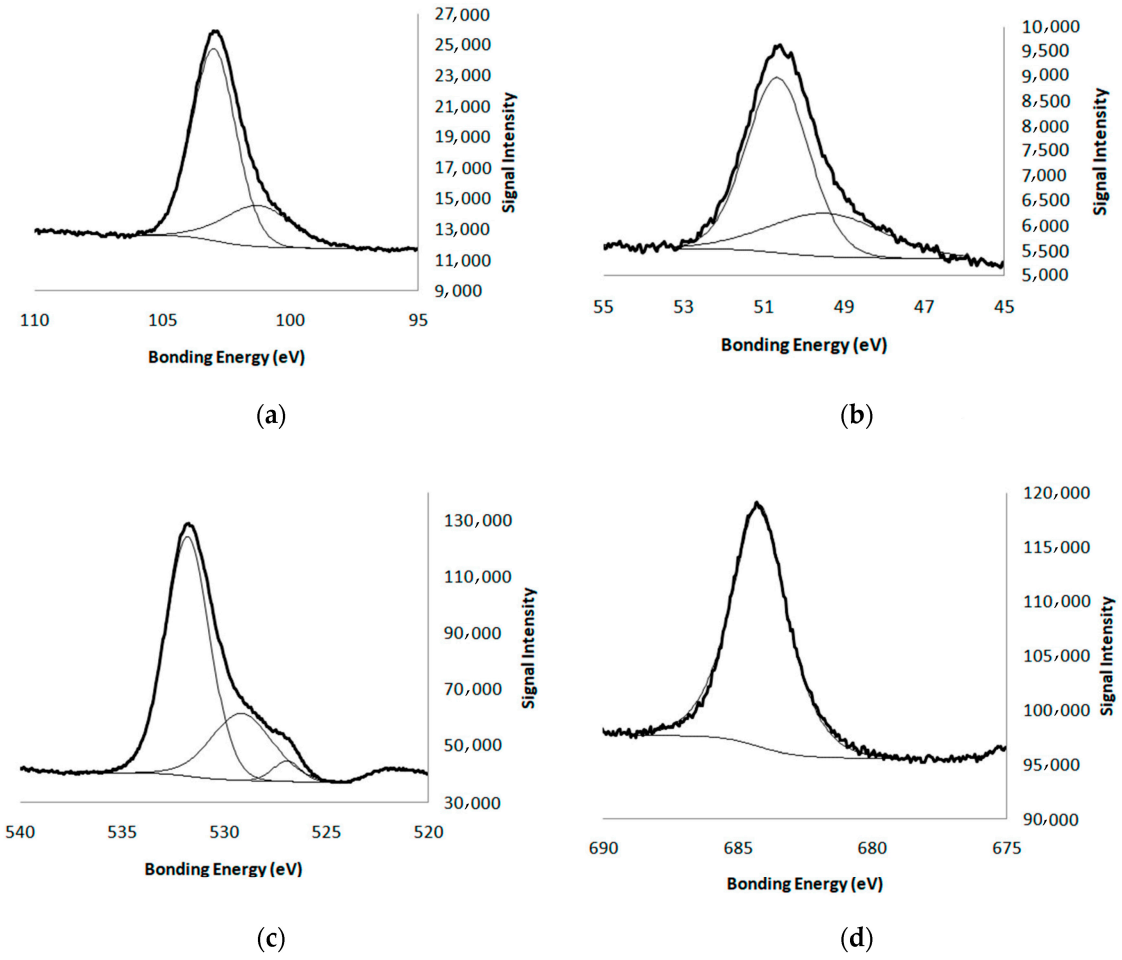

Figure 4. XPS spectra of the main elements present in the fluorohectorite: (a) Si 2p, (b) Mg 2p, (c) O 1s and (d) F 1s.

Table 3. Surface atomic concentration, binding energy and atomic ratios of elements of fluorohectorite Li-FH determined by XPS.

Atom	Mg 2p	Si 2p	Li 1s	F 1s	O 1s
%	18.8	26.7	0.0	4.7	49.8
B.E(eV)	50.6 s; 48.6 w	103 s; 101.3 w	-	684.2	531.8 s; 529.2 w
Ratios	Si/Mg		Si/O		Si/F
	1.42 (1.5 *)		0.54 (0.33 *)		5.7 (2 *)

s: strong, w: weak, * theoretical values in parenthesis.

After deconvolution, we can observe only one contribution for the F 1s peak, two contributions for Si and Mg 2p and three for O 1s. For the elements with several peak contributions, the main one was always that with the highest binding energy. No peak due to Li was observed.

The most significant information from Figure 4 and Table 3 is that O and F were present in lower amounts on the surface than the expected bulk stoichiometric values (see values *). Additionally, Li was not detected. This could be correlated with the minor peak contribution observed from deconvolution

of the Si and Mg spectra in the 2p region, with binding energies (B.E) of 101.3 and 48.6 eV, respectively, associated with higher electron density. These results could be related to an initial decomposition of hectorite with loss of Li as LiF and Li_2O. This is in agreement with the decrease of the fluorohectorite phase observed when the synthesis time was longer than 3 h. The presence of defects on surface could have a potential influence on catalysis.

The acidity of the materials, which will be used as acid catalysts for the transformation of xylose to furfural, was characterized by NH_3-TPD (Figure 5, Table 4).

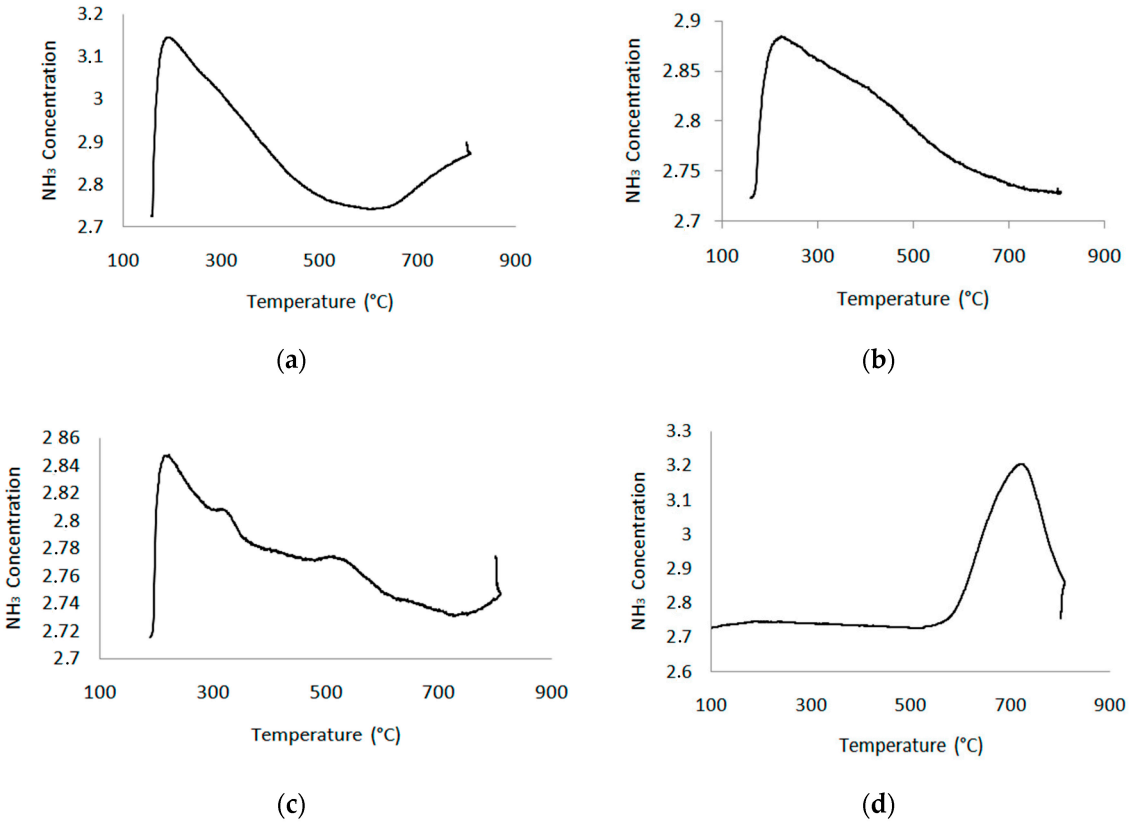

Figure 5. NH_3-TPD of catalysts: (**a**) Na-DH, (**b**) H-DH, (**c**) Li-FH, (**d**) H-FH.

Table 4. Acidity results obtained by NH_3-TPD.

Catalyst	H-β		Na-DH		H-DH		Li-FH		H-FH	
	T °C	meq/g	T °C	meq/g	T °C	meq/g	T °C	meq/g	T °C	meq/g
Acidity Strength	190	0.83	190	0.9	224	0.67	221	0.08	318	0.05
	342	0.55					316	0.09	721	0.47
							512	0.05		
							627	0.02		
Total acidity (meq/g)	1.38		0.9		0.67		0.23		0.53	
meq/m²	2.36×10^{-3}		2.7×10^{-3}		2.05×10^{-3}		14.4×10^{-3}		33.1×10^{-3}	

The temperatures indicated are those corresponding to the maximum concentration of NH_3 (meq/g) and have been calculated by integration of the area below the curve with its corresponding calibration.

By examining the acidity results of the five catalysts compared in the current study, the order of the total amount of acid sites was H-β > Na-DH > H-DH > H-FH > Li-FH (Table 4). It is important to note that for H-FH, the acidity was very strong, since the maximum of the desorption temperature for the main desorption peak was 721 °C. This confirms that fluorination increased the strength of acidity,

as expected. Additionally, although the acidity strength of H-β was higher than that observed for the hectorites Na-DH, H-DH and Li-FH, it was lower enough than that obtained for H-FH. The acidity of H-β, as described in the literature, can be assigned to Brønsted acid sites with some contribution of Lewis acid sites due to the presence of structural defects [32]. Another question to note is the higher number of acid sites of Na-DH compared to H-DH. Acidity should be mainly due to the Lewis and Brønsted acid sites. However, the acidity of H-DH was stronger than the acidity of Na-DH, since the NH_3 desorption took place at higher temperature (224 °C compared to 190 °C). The total acidity of Li-FH was the lowest, but presented several contributions, mainly due to Lewis acid sites, but probably also with a certain amount of Brønsted acid sites due to the hydrolysis of the Li^+ cation. Interestingly, fluorinated hectorites presented much higher amount of acid sites by m^2, especially H-FH, than the rest of catalysts (Table 4).

2.2. Catalytic Tests

2.2.1. Preliminary Experiments

To optimize the reaction conditions (temperature, time and xylose concentration), some preliminary studies were performed using microwave heating and H-β zeolite as catalyst. Figure 6a shows the effect of temperature (120, 140, 160 and 180 °C) on the production of furfural using biomass extract with xylose concentration of 12 g/L and toluene as co-solvent in a water:toluene volume ratio of 1:1 for 2 h. Furfural was produced in the water medium, but this medium also favored the formation of humines, which should be avoided by the extraction of furfural to the toluene phase.

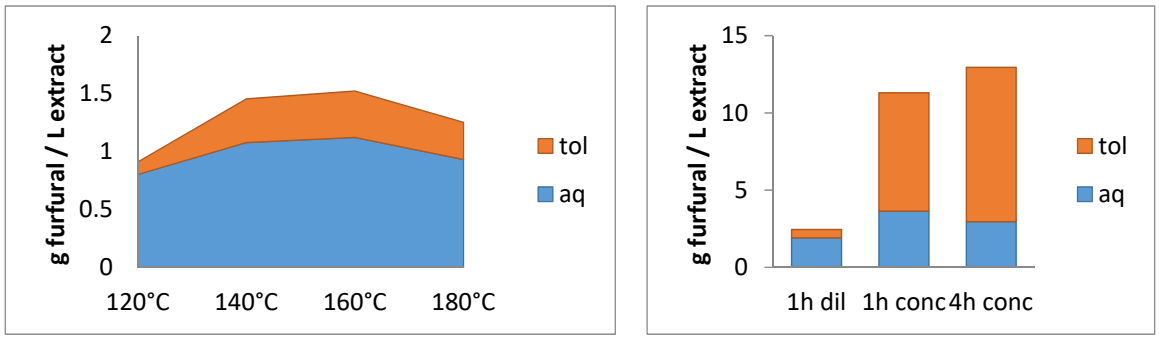

(**a**) (**b**)

Figure 6. (**a**) Effect of the reaction temperature, and (**b**) effect of the concentration of the xylose extract and reaction time on the production of furfural using H-β zeolite catalyst.

The production of furfural increased from 120 to 160 °C but decreased at 180 °C due to the formation of higher amounts of humines, probably as a consequence of the increase of the furfural amount in the medium [5]. However, the amount of furfural was always higher in the aqueous phase. To minimize the formation of humines, the reaction was performed at shorter time. The result was an increase of furfural production (2 g/L compared to 1.5 g/L), but the highest amount of furfural was again detected in the aqueous phase Figure 6b (1 h dil).

The yield of furfural was low in all cases. This can be explained by the low efficiency of furfural extraction from the aqueous phase to the toluene phase, probably due to the low concentration of xylose used in the experiments. This can make it difficult to reach equilibrium in the furfural distribution between both solvents. Higher concentrations of xylose in the extract should favor higher furfural concentrations, and at these conditions the extraction of furfural to the organic phase should be easier. Therefore, higher concentration of xylose extract and longer reaction times were tested in order to increase the extraction efficiency. Extract with a higher xylose concentration was prepared by increasing by three times the initial amount of ground almond shells. With this concentrated xylose solution (36 g/L), two experiments were performed at 160 °C, applying microwaves for 1 and 4 h, respectively.

The results are shown in Figure 6b (1 h conc and 4 h conc). The increase of the furfural production was three times higher probably due to the higher effectiveness of furfural extraction to the toluene phase, which resulted in the formation of small amounts of humines. However, longer reaction time favored the formation of greater amounts of humines.

Commercial xylose was also used as an alternative to biomass in order to avoid the homogeneous catalysis contribution and the effect of this acidity on the hectorites since the extracts obtained from almond shells were extremely acid (pH = 0.63). With this study, we aimed to establish a reliable comparison between the catalytic behavior of the hectorites synthesized. H-β zeolite was also used for comparison.

2.2.2. Effect of the Catalyst

The effect of the catalysts was studied using aqueous commercial xylose solutions (Figure 7) and acid xylose extract solutions obtained from biomass (Figure 8) at 160 °C for 1 and 4 h.

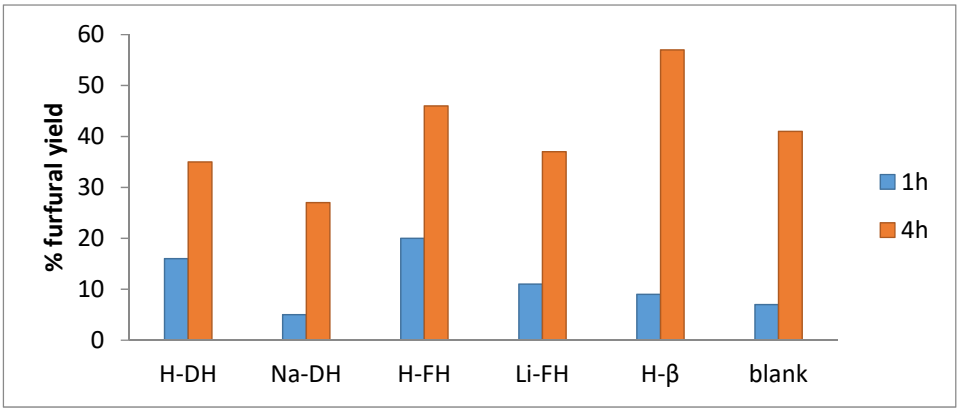

Figure 7. Furfural yields (%) using aqueous commercial xylose solutions (36 g/L) with toluene as co-solvent in a ratio of 1:1 at 160 °C for 1 and 4 h for all catalysts.

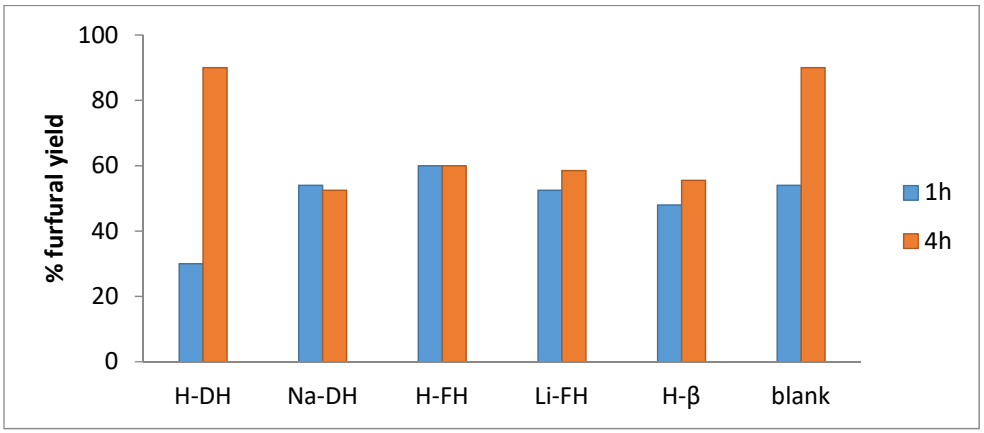

Figure 8. Furfural yields (%) using acid xylose extract solutions obtained from biomass and toluene as co-solvent in a ratio of 1:1 at 160 °C for 1 and 4 h for all catalysts.

After 1 h of reaction, the best furfural yield was obtained with the H-FH catalyst (20%). The order was H-FH > H-DH > Li-FH > H-β > blank > Na-DH. This catalytic behavior can be explained considering the amount, strength and type of acidity present in the different samples. Lewis acid sites can have some contribution to the furfural production but should be also responsible for the formation of condensation products [5]. Catalysts Na-DH, Li-FH and H-β, with the presence of Lewis acid sites, should produce higher amounts of condensation products and, therefore, the furfural yield should be lower. The catalyst with the highest amount of Lewis acid sites should be Na-DH, and, in fact,

this catalyst presented a furfural yield value similar than that of the blank (Figure 7). For H-β and Li-FH, the presence of Brønsted acidity, as previously described, can explain their position in the yield order. On the other hand, the Brønsted acid sites, which favored the formation of furfural, can explain the higher activity observed for protonated hectorites (H-FH and H-DH) when compared to Li-FH and Na-DH, respectively. H-FH was the catalyst with the strongest Brønsted acid sites, while H-DH showed weaker acidity but in higher amounts (Table 3).

When the reaction time was increased up to 4 h, the catalytic behavior was different and the order was H-β > H-FH > blank > Li-FH ≈ H-DH > Na-DH. The higher Lewis acidity of Na-DH could again explain its lower furfural yield (27%), because of the formation of condensation products. The higher yield of H-β should be related to its higher total acidity (Table 4), since, at longer time, weaker Brønsted acid sites and Lewis acid sites could participate in the furfural production [5].

In these experiments, after 1 h of reaction, the order of furfural yield values was H-FH (60) > Na-DH (54) = blank (54) ≈ Li-FH (53) > H-β (48) > H-DH (30). The furfural yields were higher when using the xylose extract obtained from biomass than when using aqueous commercial xylose solutions (Figure 8). The contribution of the homogeneous catalysis due to the acid extract could explain these higher values. The furfural yields were similar for all catalysts but slightly higher for H-FH (60%). This can be related to its stronger Brønsted acid sites. In contrast, the less active catalytic system was H-DH. Some solubilization of Mg^{2+} and Li^{+} of the hectorite structure due to the acidity of the extract solution, which involved the generation of defects in the structure, together with some exchange between the interlamellar ions and the protons from the extract (reducing the weight of homogeneous catalysis) could explain these results. In order to check this, pH was measured before and after reaction. In blank reactions, no variation was observed, but when solid catalysts were used, pH increased from +0.10 (with H-β) to +0.25 (with Li-FH). These differences should be related to modifications in the solid catalysts due to the acidic medium. Therefore, after 1 h of reaction, there was a decrease of the contribution of the homogeneous Brønsted catalysis, while the contribution of the heterogeneous Brønsted acid catalysis competed with the new Lewis acid sites generated by the partial destruction of the structure of the materials, together with a proton exchange process due to the acid extract.

Regarding the catalytic results obtained at a longer reaction time (4 h), we can consider two groups of catalysts: (1) the blank and H-DH with a furfural yield of 90%, and (2) the rest of catalysts, which had similar furfural yields (52–60%). Considering that, after 1 h of reaction, catalyst H-DH was the least active, we think that at longer reaction times, Brønsted acid sites together with new Lewis acid sites in the H-DH catalyst could compensate the loss of acidity in the homogeneous system. For this reason, the furfural yield was similar to that obtained with the blank. For the rest of catalysts, the catalytic results were similar to those obtained after 1 h of reaction. The modifications in solid catalysts and the pH increase in the homogeneous medium seem to favor humines formation. Structural information about catalyst modifications after reaction was obtained by XRD.

The XRD pattern of the catalyst H-FH after 4 h of reaction using a concentrated xylose extract (Figure 9) showed the presence of the expected peaks corresponding to fluorohectorite (001, 004). Additionally, a broad peak at around $2\theta = 22^{\circ}$ appeared. This peak could be related to: (1) amorphous SiO_2 obtained by partial destruction of the clay by the solubilization of Mg and Li, and/or (2) amorphous organic material covering the clay surface. This means that the lamellar structure of clays was partially preserved but covered by the humines produced during the reaction. This can explain the loss of activity observed for this catalyst from 1 to 4 h. This behavior could also be expected for the rest of the solid acid catalysts.

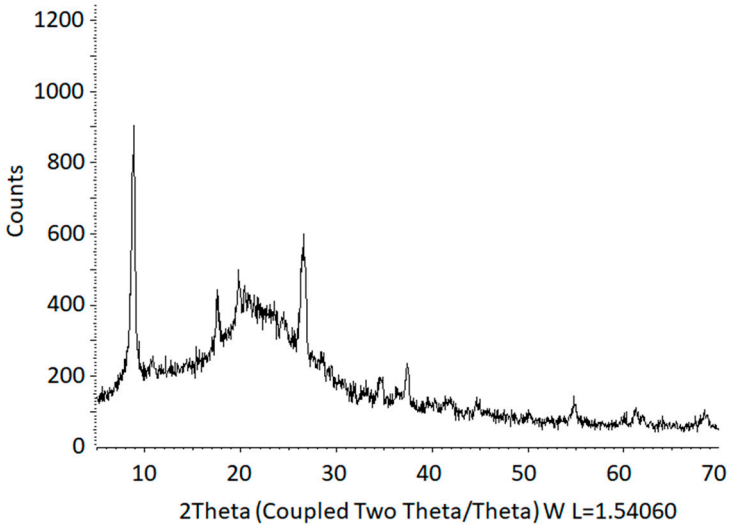

Figure 9. XRD pattern of the recovered H-FH after the catalytic reaction.

3. Materials and Methods

A new method for the synthesis and purification of fluorohectorites was developed. Delaminated hectorite, protonated delaminated hectorite and protonated fluorohectorite were prepared and compared with protonated beta-zeolite for the acid-catalyzed reaction studied.

3.1. Materials

MgO, SiO_2 and xylose were supplied by Sigma Aldrich, LiF by Acros Oganics, MgF_2 by Alfa Aesar, and H_2SO_4, butanol and toluene by Scharlau. NH_4β-zeolyte was supplied by zeolyst, NH_4NO_3 by Carlo Erba and ethanol by Panreac Applichem. The powder of almond shells was obtained from UNIO Cooperative in Reus (Tarragona).

3.2. Fluorohectorite Preparation

Several lithium fluorohectorites were synthesized according to Barrel and Jones, who used two main routes, as described above [30]. Thus, we prepared two groups of fluorohectorites: one group by solid-state reaction at 800 °C, and the other group in liquid phase at 850 °C.

The group of fluorohectorites prepared at 800 °C (FH800s), with formula $Li_{0.7}[(Mg_{5.3}Li_{0.7})Si_8O_{20}F_4]$, was synthesized by mixing sintered SiO_2, sintered MgO, commercial LiF and commercial MgF_2 in a 8:4:2:2 molar ratio, respectively. Sintered MgO and SiO_2 were obtained by heating their corresponding commercial compounds at 800 °C for 1 h in a conventional muffle furnace. For the group of samples prepared at 850 °C (FH850ns), commercial LiF, commercial MgO and commercial SiO_2 were mixed in a 12:4:8 molar ratio, respectively, to obtain fluorohectorites with formula $Li_{1.16}[(Mg_{4.84}Li_{1.16})Si_8O_{20}F_4]$. In all cases, the mixture was homogenized following a sequence of different methods: grounding, suspending in acetone under an ultrasounds bath (Selecta) for 20 min, and finally evaporating the solvent and drying the solid in an oven at 80 °C overnight. The resulting solid was then heated in a conventional muffle furnace at 850 °C or 800 °C for different times to study the evolution of the reaction (3, 6, 12 and 24 h at 800 °C and 0.5, 1 and 2 h at 850 °C).

The sample with the highest amount of fluorohectorite phase was purified. To do this, the solid was suspended in water and stirred overnight at room temperature. Finally, the suspension was centrifuged at 600 rpm for 6 min, the liquid phase was then re-centrifuged at 4000 rpm for 30 min, and the solid obtained was stored and characterized. The purified fluorohectorite was called Li-FH.

3.3. Catalyst Preparation

Na^+ delaminated hectorite (Na-DH) was synthesized following a method previously developed by our research group using trimethyldodecylammonium chloride as template [27].

H^+ delaminated hectorite (H-DH) and H^+ Fluorohectorite (H-FH) were prepared by ionic exchange of previously synthesized Na-DH and Li-FH, respectively, with 1 M NH_4NO_3 aqueous solution by refluxing for 1 h. Then, the suspension was centrifuged and the resulting solid was calcined at 540 °C for 3 h and stored.

Protonated Beta zeolite (H-β) was obtained from calcination of commercial β-NH_4^+ zeolite at 540 °C for 2 h.

3.4. Characterization and Analytic Techniques

The cation exchange capacity (C.E.C.) values were determined as reported by Bergaya and Vayer (1997) [33]. Samples were dried overnight at 200 °C before measurement. For the samples prepared with the template, since the calcination procedure used for removing the template involves decomposition of the interlamellar NH_4^+ cation, before C.E.C. measurement, the samples were submitted to an exchange step with saturated NaCl solution for 36 h, washed several times with deionized water, and dried.

Surface area was measured by nitrogen physisorption using a Quadrasorb SI surface analyzer. Samples were degassed under vacuum at 110 °C overnight before measurements. Specific surface areas were determined from BET method. Pore size distribution was predicted from the desorption wing of the isotherm by applying the BJH method.

XRD (X-Ray Diffraction) patterns were obtained using a Siemens D5000 diffractometer (Bragg–Brentano parafocusing geometry and vertical θ–θ goniometer) fitted with a curved graphite diffracted-beam mono chromator and diffracted-beam Soller slits, a 0.06° receiving slit, and scintillation counter as a detector. The angular 2θ diffraction range was between 2 and 70°. Sample was dusted on to a low background Si (510) sample holder. The data were collected with an angular step of 0.05° at 3 s per step and sample rotation. Cukα radiation was obtained from a copper X-ray tube operated at 40 kV and 30 mA. The JCPDS files used for identification of the crystalline phases were 01-075-0909(C) for antophyllite and 01-073-5680(N) for fluorohectorite.

The total surface acidity of the catalyst precursors was determined by NH_3-TPD conducted on AC2920 apparatus. In a typical experiment, about 0.2 g sieved catalyst precursor was loaded in U-shaped quartz tube and submitted to surface pre-treatment under He flow at 350 °C for 1 h. It was then cooled down to 100 °C and saturated with NH_3 for 30 min. The physically adsorbed NH_3 was removed by purging the sample with pure He for 30 min. After that, the sample was heated from 100 to 800 °C at 10 °C/min. The NH_3 desorption was monitored with a TCD detector. The peak area of the TPD peaks was correlated with the amount of desorbed NH_3 on the basis of pulsed NH_3 injection experiment. The total surface acidity was calculated from the amount of ammonia desorbed.

Transmission electron micrographs (TEM) of the samples were obtained with a JEOL 1011 transmission electron microscope operating at an accelerating voltage of 100 kV and magnification of 80 k. Samples were prepared by dispersing 0.1 mg of clay in 50 μL ethanol and applying a drop of the resulting suspension onto a carbon coated-copper grid.

Energy Dispersive X-Ray (EDX) of fluorohectorite was performed on a scanning electron microscope, JEOL JSM6400, operating at accelerating voltage of 15 kV and working distances of 15 mm. All samples were covered with a graphite layer. Accumulation time was 120 s. Surface Si, Mg and F contents were quantified.

X-ray Photoelectron Spectroscopy (XPS), which was used for the surface characterization of the purified fluorohectorite, was performed with a SPECS system equipped with an Al anode XR50 source operated at 150 W and a Phoibos MCD-9 detector. The pressure in the analysis chamber was kept below 10^{-7} Pa. The area analyzed was approximately 2 mm × 2 mm. The pass energy of the hemispherical analyzer was set at 25 eV, and the energy step was fixed at 0.1 eV. Powdered samples were pressed to self-supported pellets. Data processing was carried out with the Casa XPS

program (Casa Software Ltd., Teignmouth, UK). The BE values were referenced to the C1s peak at BE = 284.8 eV. Atomic fractions were calculated using peak areas normalized from the acquisition parameters after background subtraction, experimental sensitivity factors, and transmission factors provided by the manufacturer.

The reaction products of the catalytic reaction were analyzed by gas chromatography in a Shimadzu GC-2010 using a 60 m SupraWAX280 column, and following the temperature program of 2 min at 100 °C followed by 10 °C/min until 250 °C and 6 min at 250 °C to identify furfural.

3.5. Extraction of Xylose from Biomass

5 or 15 g of grounded almond shells were suspended in 50 mL of 1% (m/v) H_2SO_4 solution under magnetic stirring in a microwave Teflon reactor. Then, the reaction mixture was heated using microwaves up to 120 °C for 1 h. The microwaves equipment was a Milestone Ethos Touch control laboratory apparatus working at frequency of 2.45 GHz and equipped with controller temperature. The irradiation microwave was programmed to work at a maximum of 400 W. The solid product was filtered, and the liquid phase was stored as "extract" in the fridge. The average concentrations of xylose for both extract solutions were 12 g/L for the 5 g extract, and 36 g/L for the 15 g extract. The xylose concentration was determined by HPLC chromatography with a RI detector using a Rezex RHM-Monosaccharide H^+ (8%) column.

3.6. Catalytic Reaction

25 mL of extract or aqueous solutions of xylose together with 25 mL of toluene were added to a 80 mL microwave Teflon reactor. Then, the corresponding catalyst was added to the liquid mixture in a proportion of 6.24 g of catalyst per L of aqueous solution. The closed reactor was heated under microwaves (400 W) at different temperatures (120, 140, 160 and 180 °C) for different times (1, 2, 4 h). Finally, the different phases obtained were filtered and analyzed by gas chromatography. The retention time for furfural was 12.1 min.

The yield of furfural was calculated using the following formula:

$$\text{Yield}(\%) = \frac{\text{moles of furfural obtained}}{\text{theoretical moles of furfural}} \times 100$$

When biomass extract was used as reagent, the theoretical moles of furfural were calculated by assuming the average xylose value for each single extract.

4. Conclusions

A new methodology for preparing crystalline fluorohectorite was developed. The presence of F was involved in a significant increase in the acidity strength for the protonated form, H-FH. The total acidity by m^2 of H-FH, calculated from NH_3-TPD studies, was 33.1×10^{-3} meq NH_3/m^2, fourteen times higher than that obtained for the zeolite H-β, which was used as reference acid catalyst. H-FH was the most efficient catalyst at shorter reaction times (1 h) for the transformation of xylose to furfural independently of whether xylose was commercial or produced from almond shells, resulting in furfural yields of 20% and 60%, respectively. The stronger Brønsted acidity of the protonated fluorohectorite favored a faster production of furfural at these conditions. This behavior confirms the high potential for this cheap and easy-to-synthesize material to be used, in general, as an acid catalyst. On the other hand, after 4 h of reaction, the best furfural yields were 57% and 90% using commercial xylose and biomass extract, respectively, with the H-β zeolite in the first case, and with the blank and H-DH catalyst in the second case. The higher total acidity of H-β can explain this result without the contribution of acid homogeneous catalysis, since weaker Brønsted and Lewis acid sites could slowly catalyze the furfural production with time. When using the biomass extract, the interpretation was more complex regarding the acid homogeneous catalysis contribution and the action of the acid medium on the solid

catalysts. Hectorites have interesting acid properties that can be applied in catalysis, but the presence of mineral acids in the reaction medium should be avoided.

Author Contributions: This study was conducted through contributions of all authors. Conceptualization, P.S. and Y.C.; Funding acquisition, P.S. and Y.C.; Investigation, V.S.; Methodology, V.S., A.D., P.S. and J.L.; Supervision, P.S. and Y.C.; Writing—original draft, V.S., P.S. and Y.C.

Funding: This research was funded by Ministerio de Economía y Competitividad of Spain and European Regional Development Funds [CTQ2015-70982-C3-3-R].

Acknowledgments: The authors acknowledge the recognition obtained from the Generalitat de Catalunya [2017 SGR 798 and 2017 SGR 128].

Conflicts of Interest: The authors declare no conflict of interest.

References

1. Nakagawa, Y.; Tamura, M.; Tomishige, K. Catalytic conversions of furfural to pentanediols. *Catal. Surv. Asia* **2015**, *19*, 249–256. [CrossRef]
2. Qing, Q.; Guo, Q.; Zhou, L.; Wan, Y.; Xu, Y.; Ji, H.; Gao, X.; Zhang, Y. Catalyitc conversion of corncob and corncob pretreatment hydrolysate to furfural in a biphasic system with addition of sodium chloride. *Biores. Tech.* **2017**, *226*, 247–254. [CrossRef]
3. Nakagawa, Y.; Tamura, M.; Tomishige, K. Catalytic reduction of biomass-derived furanic compounds with hydrogen. *ACS Catal.* **2013**, *3*, 2655–2668. [CrossRef]
4. Cai, C.M.; Zhang, T.; Kumar, R.; Wyman, C.E. Integrated furfural production as a renewable fuel and chemical platform from lignocellulosic biomass. *J. Chem. Technol. Biotechnol.* **2014**, *89*, 2–10. [CrossRef]
5. Weingarten, R.; Tompsett, G.; Conner, W.; Huber, G. Design of solid acid catalysts for aqueous-phasedehydration of carbohydrates: The role of Lewis and Brønsted acid sites. *J. Catal.* **2011**, *279*, 174–182. [CrossRef]
6. Choudhary, V.; Sandler, S.; Vlachos, D. Conversion of xylose to furfural using lewis and brønsted acid catalysts in aqueous media. *ACS Catal.* **2012**, *2*, 2022–2028. [CrossRef]
7. Karinen, R.; Vilonen, K.; Niemelä, M. Biorefining: Heterogeneously catalyzed reactions of carbohydrates for the production of furfural and hydroxymethylfurfural. *ChemSusChem* **2011**, *4*, 1002–1016. [CrossRef]
8. Bhaumik, P.; Dhepe, P.L. Exceptionally high yields of furfural from assorted raw biomass over solid acids. *RSC Adv.* **2014**, *4*, 26215–26221. [CrossRef]
9. Ji, L.Q. An assessment of agricultural residue resources for liquid biofuel production in China. *Renew. Sust. Energy Rev.* **2015**, *44*, 561–575. [CrossRef]
10. Dias, A.S.; Pillinger, M.; Valente, A.A. Liquid phase dehydration of d-Xylose in the presence of Keggin-type heteropolyacids. *Appl. Catal. A Gen.* **2005**, *285*, 126–131. [CrossRef]
11. Dias, A.S.; Lima, S.; Carriazo, D.; Rives, V.; Pillinger, M.; Valente, A.A. Exfoliated titanate, niobate and titanoniobatenanosheets as solid acid catalysts for the liquid-phase dehydration of d-Xylose into furfural. *J. Catal.* **2006**, *244*, 230–237. [CrossRef]
12. Lima, S.; Pillinger, M.; Valente, A.A. Dehydration of d-Xylose into furfural catalysed by solid acids derived from the layered zeolite Nu-6(1). *Catal. Commun.* **2008**, *9*, 2144–2148. [CrossRef]
13. Qi, X.; Watanabe, M.; Aida, T.M.; Smith Jr, R.L. Catalytic dehydration of fructose into 5-hydroxymethylfurfural by ion-exchange resin in mixed-aqueous system by microwave heating. *Catal. Commun.* **2008**, *10*, 799–805. [CrossRef]
14. Qi, X.; Watanabe, M.; Aida, T.M.; Smith, R.L. Catalytical conversion of fructose and glucose into 5-hydroxymethylfurfural in hot compressed water by microwave heating. *Catal. Commun.* **2008**, *9*, 2244–2249. [CrossRef]
15. Yemis, O.; Mazza, G. Acid-catalyzed conversion of sylose, xylan and straw into furfural by microwave-assisted reaction. *Biores. Tech.* **2011**, *102*, 7371–7378. [CrossRef]
16. Yemos, O.; Mazza, G. Catalytic performances of various solid catalysts and metal halides for microwave-assisted hydrotermal conversion of xylose, xylan, and straw to furfural. *Waste Biomass Valorization* **2019**, *10*, 1343–1353. [CrossRef]

17. Gómez Millán, G.; El Assal, Z.; Nieminen, K.; Hellsten, S.; Llorca, J.; Sixta, H. Fast furfural formation from xylose using solid acid catalysts assisted by a microwave reactor. *Fuel Process. Technol.* **2018**, *182*, 56–67. [CrossRef]
18. Delbecq, F.; Wang, Y.; Len, C. Conversion of xylose, xylan and rice husk into furfural via betaine and formic acid mixture as novel homogeneous catalyst in biphasic system by microwave-assisted dehydration. *J. Mol. Catal. A Chem.* **2016**, *423*, 520–525. [CrossRef]
19. Le Guenic, S.; Gergela, D.; Ceballos, C.; Delbecq, F.; Len, C. Furfural production from d-xylose and xylan by using stable nafion nr50 and nacl in a microwave-assisted biphasic reaction. *Molecules* **2016**, *21*, 1102. [CrossRef]
20. Wang, Y.; Delbecq, F.; Kwapinski, W.; Len, C. Application of sulfonated carbon-based catalyst for the furfural production from d-xylose and xylan in a microwave-assisted biphasic reaction. *Mol. Catal.* **2017**, *438*, 167–172. [CrossRef]
21. Wang, Y.; Delbecq, F.; Varma, R.S.; Len, C. Comprehensive study on expeditious conversion of pre-hydrolyzed alginic acid to furfural in Cu(II) biphasic systems using microwaves. *Mol. Catal.* **2018**, *445*, 73–79. [CrossRef]
22. Delbecq, F.; Takahashi, Y.; Kondo, T.; Corbas, C.C.; RuizRamos, E.; Len, C. Microwave assisted efficient furfural production using nano-sized surface-sulfonated diamond powder. *Catal. Commun.* **2018**, *110*, 74–78. [CrossRef]
23. Xiouras, C.; Radacsi, N.; Sturm, G.; Stefanidis, G.D. Furfural Synthesis form D-Xylose in the Presence of Sodium Chloride: Microwave versus Conventional Heating. *ChemSusChem* **2016**, *9*, 20159–20166. [CrossRef]
24. Conner, W.C., Jr.; Tompsett, G.A. How Could and Do Microwaves Influence Chemistry at Interfaces? *J. Phys. Chem. B* **2008**, *112*, 2110–2118. [CrossRef]
25. Lourvanij, K.; Rorrer, G.L. Reaction Rates for the Partial Dehydration of Glucose to Organic Acids in Solic-Acid, Molecular-Sieving Catalyst Powders. *J. Chem. Technol. Biotechnol.* **1997**, *69*, 35–44. [CrossRef]
26. Lourvanij, K.; Rorrer, G.L. Dehydration of glucose to organic acids in microporous pillared clay catalysts. *Appl. Catal. A Gen.* **1994**, *109*, 147–165. [CrossRef]
27. Sánchez, T.; Salagre, P.; Cesteros, Y.; Bueno-López, A. Use of delaminated hectorites as supports of copper catalysts for the hydrogenolysis of glycerol to 1,2-propanediol. *Chem. Eng. J.* **2012**, *179*, 302–311. [CrossRef]
28. Majid, A.; Argue, S.; Kingston, D.; Lang, S. Controlled fluorination of clays. *J. Fluor. Chem.* **2007**, *128*, 1012–1018. [CrossRef]
29. Kalo, H.; Möller, M.W.; Kunz, D.A.; Breu, J. How to maximize the aspect ratio of clay nanoplatelets. *Nanoscale* **2012**, *4*, 5633–5639. [CrossRef]
30. Barrer, R.M.; Jones, D.L. Chemistry of Soil Minerals. Part VIII. Synthesis and Properties of Fluorhectorites. *J. Chem. Soc. A* **1970**, 1531–1537. [CrossRef]
31. Sing, K.S.W.; Everett, D.H.; Haul, R.A.W.; Moscou, L.; Pierotti, R.A.; Rouquerol, J.; Siemieniewska, T. Reporting physisorption data for gas/solid systems with special reference to the determination of surface area and porosity. *Pure Appl. Chem.* **1985**, *57*, 603–619. [CrossRef]
32. Marques, J.P.; Gener, I.; Ayrault, P.; Bordado, J.C.; Lopes, J.M.; Ribeiro, F.R.; Guisnet, M. Dealumination of HBEA zeolite by steaming and acid leaching: distribution of the various aluminic species and identification of the hydroxyl groups. *C. R. Chimie* **2005**, *8*, 399–410. [CrossRef]
33. Bergaya, F.; Vayer, M. CEC of clays: measurement by adsorption of a copper ethylenediamine complex. *Appl. Clay Sci.* **1997**, *12*, 275–280. [CrossRef]